From climate predictions to flood risk assessment for a portfolio of structures

F. Jalayer, R. De Risi, G. Manfredi
Department of Structures for Engineering and Architecture, University of Naples Federico II, Naples, Italy

F. De Paola, M. E. Topa, M. Giugni
Department of Civil, Architectural and Environmental Engineering, University of Naples Federico II, Naples, Italy

E. Bucchignani
Centro Mediterraneo sui Cambiamenti Climatici (CMCC)

E. Mbuya, A. Kyessi
Institute of Human Settlements Studies (IHSS), Ardhi University, Dar es Salaam, Tanzania

P. Gasparini
Analysis and Monitoring of Enviromental Risk (AMRA)

ABSTRACT: Assessment and prediction of the adverse effects of the climate-related events, quantification of the vulnerability of the affected areas and risk assessment are important steps in an integrated climate change adaptation strategic decision-making procedure. This work presents a probabilistic performance-based procedure for flood risk assessment for the structures in a portfolio of spatially-distributed structures in a detailed micro-scale. This methodology has its starting point in the down-scaling of global climate projections for a prescribed climate scenario and historical data as far as it regards the rainfall intensity, duration and frequency. The risk is expressed in terms of the annual rate (and probability) of exceeding a structural limit state, expected replacement cost and expected number of people endangered by the flooding (hypothesis of no evacuation). This procedure is described through an application for Suna, a subward of Magomeni in Dar es Salaam City (Tanzania), located in the Msimbazi river basin, having a high concentration of informal settlements.

1 INTRODUCTION

Hydro-meteorological or climate-related hazards, such as storms, droughts, floods and landslides, transform into natural disasters when they hit vulnerable areas. In the last decades, climate-related disasters alone accounted for between 70-90 percent of the natural disasters around the globe (Hoyois and Guha-Sapir, 2012). On the other hand, the rapid rate of urbanization leads to an increase the exposure to risk in urban areas. It is sufficient to highlight that around half of the world's population lives in urban areas at present; by 2050, this ratio is estimated to rise up to around 70% (UN-HABITAT, 2010). There is increasing evidence in the favor of a correlation between the climate change and extreme weather-related phenomena (Khan and Kelman, 2011). In this regard, assessment and prediction of the adverse effects of climate change scenarios on the frequency and/or intensity of extreme weather-related events and delineation of the potentially vulnerable areas are important steps in an integrated climate change adaptation strategy.

In the recent years, increasing attention is focused on flooding risk assessment. In fact, several publications discuss the consequences of flooding, such as loss of life (Jonkman et al., 2008), economic losses (Pistrika and Tsakiris, 2007), and damage to buildings (Smith, 1994, Kelman, 2002, Kang et al., 2005, Schwarz and Maiwald, 2012). These research efforts have many aspects in common, such as a direct link between the flooding intensity and the incurred damage, and that they are based on real damage observed in the aftermath of the flooding event. On the other hand, many research efforts are starting to galvanize in the direction of proposing analytical models for flood vulnerability assessment taking into account the many sources of uncertainties. For instance, Nadal et al. (Nadal et al., 2009) propose a stochastic method for the assessment of the direct impact of flood actions on buildings.

This work presents a probabilistic performance-based procedure for predicting the flooding risk for the structures in a portfolio of spatially-distributed structures in a detailed micro-scale taking into account both observed and projected rain-fall extremes. This procedure is developed in the context of the European FP7 project Climate Change and Urban Vulnerability in Africa (CLUVA). The probability-based methodology presented herein is developed for flood risk assessments for the informal settlements in the African urban settings/contexts. This procedure has a modular structure and consists of climate modeling/flood hazard assessment, portfolio vulnerability assessment and risk assessment. The flood risk assessment is done for alternative one-year time windows, namely, 2010-2011 (based on observed rainfall data) and 2050-2051 (based on observed rainfall data and rainfall projections).

The application of this methodology is presented for the informal settlements in a flood-prone neighborhood in Dar es Salaam (DSM), Tanzania, Africa.

2 CLIMATE MODELING AND FLOOD HAZARD ASSESSMENT

Flood hazard is expressed herein as the annual probability of exceeding a specific flooding height (h_f). In the first place, the rainfall probability curve or the rainfall Intensity-Duration-Frequency (*IDF*) curve is extracted from the historical data or from down-scaling of regional climate projections. The *IDF* curve is employed next as the input of a catchment rainfall-runoff model in order to determine the hydrograph and the peak discharge. This information, together with detailed cartography of the zone and a digital elevation model is used as input into the hydraulic model in order to calculate the inundation profile. The results can be presented in terms of the annual rate/probability of exceeding a specific value of flooding height and flooding velocity for the nodes of a lattice covering the interest zone.

2.1 *Historical rainfall data*

The riverine flooding events are strictly connected to rainfall patterns. Therefore, the rainfall data time-series are essential pieces of information for determining the total flooding discharge. They can be obtained as pluviometric time-series from governmental organizations and/or internet sources (e.g., www.tutiempo.net and www.knmi.nl). It is desirable that the pluviometric data are available as precipitation extremes (maxima) recorded over a range of time intervals. The rainfall maxima recorded for different intervals are used in order to construct the rainfall IDF curve (described in detail later). The rainfall time-series can be also used to evaluate the antecedent soil moisture condition (AMC). In hydrological modeling, antecedent moisture condition is usually associated with the pre-storm soil moisture deficit. This latter has a significant effect on the amount of rainfall drained by the river network and finally on the flooding potential of a rainstorm.

2.2 *Climate projections*

Future climate patterns may manifest adverse effects on the frequency and/or intensity of extreme weather-related events such as floods.

In compliance with the Intergovernmental Panel on Climate Change (IPCC) scenarios (Alley et al., 2007), climate projections are generally evaluated using General Circulation Model (GCM). A GCM is a mathematical model that simulates the general atmospheric and oceanic circulation using a specific

formulation of the Navier-Stockes equations, discretized with spatial resolutions in the order of 100 km.

Ideally, GCMs can be used to produce long-term simulations to be used for catastrophe modeling. However, for a realistic simulation of precipitation patterns, representing the vertical structure of the atmosphere as well as the effect of the terrain on atmospheric circulation, a model must have a resolution less than 100 km. This is not practical since the calculation time increases exponentially. Therefore, using a GCM for direct simulation of precipitations is not feasible. Moreover, the GCMs are based on simplified microphysics and may not provide a solid representation of precipitation in the mountainous areas (Bellucci et al., 2012).

The application of a Regional Climate Model (RCM) with horizontal spatial resolution of about 10 km can be useful for the description of the climate variability in the local scale. A RCM depends on the definition of boundary conditions that can be obtained based on the results of a GCM. Finally, through statistical downscaling it is possible to obtain climatological data for finer spatial resolutions, in the order of 1 km. This provides the precipitation data necessary for comprehensive flood modeling.

The climate projections used in this work are provided by the CMCC (Centro Euro-Mediterraneo sui Cambiamenti Climatici). They have been obtained by following the IPCC 20C3M protocol for the 20th Century, and using RCP4.5 and RCP8.5 radiative forcing emission scenarios developed in the framework of the 5th Coupled Model Intercomparison project (WCRP, 2008).

CMCC has performed a set of climate simulations over the time period 1950-2050 with the global model CMCC-MED (Gualdi et al., 2013) (spatial resolution 80 km) in the context of the FP7 project CLUVA. The initial conditions have been obtained from an equilibrium state reached by integrating the model for 200 years with constant greenhouse gas (GHG) concentrations corresponding to 1950's. Once the climate model reaches equilibrium with the prescribed constant radiative forcing (GHG and aerosol concentrations), the simulations have been conducted by increasing the GHG and aerosol concentrations in line with observed data. These simulations have been downscaled to a spatial resolution of 8 km with the non-hydrostatic RCM COSMO-CLM (Rockel et al., 2008), developed considering the spatial extent covered by the urban area of interest. The results were further downscaled to a spatial resolution of 1 km by using a stochastical downscaling technique (Rebora et al., 2006) in order to render them suitable for modeling of precipitation patterns.

In this work, the climate projections based on the RCP8.5 scenario and downscaled to 1km resolution are taken into account. This may be considered a

worst-case scenario in terms of gas emissions and temperature increase.

2.3 Rainfall curve: historical data and climate projection

Climate modeling constitutes the first step in developing a probabilistic inundation model. Its output is usually expressed in terms of rainfall scenarios for various return periods (T_R), also known as the rainfall curves or the Intensity-Duration-Frequency (*IDF*) curves. The *IDF* curves are normally used, in lieu of sufficient data for direct probabilistic discharge modeling, in order to evaluate the peak discharge. In particular the *IDF* curves present the probability of a given rainfall intensity and duration expected to occur in a particular location. The rainfall curve is calculated herein based on both historical data and a specific climate projection scenario. The historical rainfall data (H) span from 1958 to 2010 and the climate projection (CC) is provided from 2010 to 2050.

The historical rainfall data is obtained from a single meteorological station located in the DSM International Airport at 55 meter altitude from the sea level, 6°86' latitude and 39°20' longitude. For consistency, the projection data are calculated for the same point.

Rainfall height h_r is calculated as the maximum rainfall depth in millimeters calculated in a time-window of duration d.

The annual rainfall extremes are then calculated for various time window durations. Figure 1(a) and (b) shows the two rainfall height maxima time-series used herein for d=24hr.

The first time-series depicted in Figure 1(a) is based on historical data only (hereafter referred to as H, 1958-2010). The second time-series shown in Figure 1(b), and hereafter referred to as CC, consists of (H, 1958-2010) plus climate projections for (2011-2050). A Gumble extreme-value distribution is used to describe the annual rainfall height maxima in both cases CC and H (Figure 2).
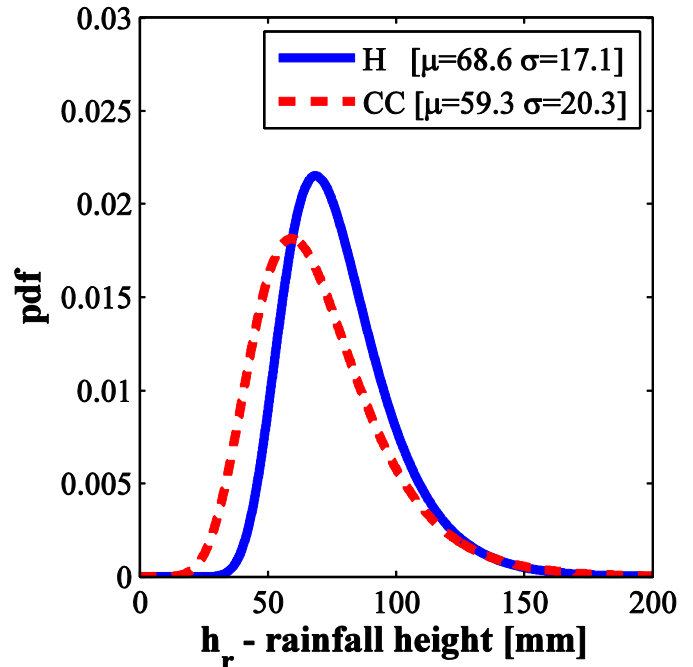
Figure 2. Probability density function for the maximum rainfall height for a duration of 24 hours.

It is worth noting that considering the climate change effects leads to a reduction of 14% in the mean rainfall height.

2.4 Rainfall curve based on incomplete records

The maximum annual rainfall data for a specific duration are not always available. In such cases, available data could be disaggregated to the desired durations. This involves generating synthetic sequences of rainfall for smaller time windows (e.g., 10', 30', 1h, 3h, 6h, 12h), with statistical properties equal to that of the observed daily rainfall. In this work, two alternative downscaling techniques are used in order to generate maximum rainfall values for the desired time windows. The short-time intensity disaggregation method (Connolly et al., 1998) has been used for simulation of smaller time windows (i.e., 10', 30', 1h) and the random cascade-based disaggregation method (Güntner et al., 2001, Olsson, 1998) has been used for larger time windows (i.e., 3h, 6h and 12h).

2.5 The results for DSM

The *IDF* curve obtained based on historical data (H) is characterized by the following relationship:

Figure 1. The annual rainfall height maxima (a) H and (b) CC for a duration of 24 hours (DSM, Airport Station).

$$h_r\left(d, T_R\right) = K_{T_R} \cdot 36.44 \cdot d^{0.25} \tag{1}$$

where $h_r(d, T_R)$ is the maximum annual rainfall height measured over a time-window of duration d, corresponding to a return period of T_R; K_{T_R} is the growing factor and is a function of the coefficient of variation for the corresponding Gumbel probability distribution. The projected *IDF* curve (CC) is obtained through the same procedure, based on the climate change projection for scenario RCP8.5 (which is a worst-case scenario reflecting increased emissions of greenhouses gasses in the atmosphere) with a spatial resolution of 80 km, spatially downscaled to a resolution of 1 km. It is characterized by the following relationship:

$$h_r\left(d, T_R\right) = K_{T_R} \cdot 31.70 \cdot d^{0.26} \tag{2}$$

Table 1 reports the values of the growing factor K_{T_R} for various return periods based on the historical data (H) and climate projections (CC).

Table 1. Growing factors for the different return periods

TR	2Ys	10Ys	30Ys	50Ys	100Ys	300Ys
H	0.95	1.42	1.70	1.83	2.01	2.29
CC	0.94	1.50	1.84	2.00	2.21	2.41

The rainfall curves for CC and H for 2 different return periods are plotted in Figure 3.
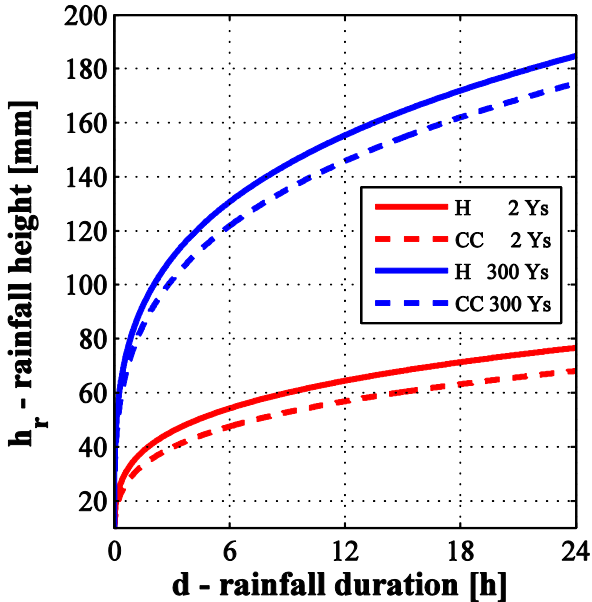
Figure 3. IDF curves related to return period of 2 Years and 300 Years for CC and H.

It is possible to observe that for DSM city, this climate scenario leads to a decrease in terms of rainfall intensity. In fact, the IDF curves that take into account the climate projection (the dotted lines in Figure 3) are lower than those evaluated based on historical data series (the solid line in Figure 3). Nevertheless, although the flooding intensity considering the projections decreases with respect to the

historical data, the growing factor demonstrates a slight increase (Table 1). As mentioned before, the growing factor is a function of the coefficient of variation for the extreme value distribution. Having a higher coefficient of variation (with constant mean or central value) leads to higher probability for extreme rainfall events (i.e., in the tail of the distribution).

2.6 *Antecedent Moisture Conditions*

Antecedent Moisture Condition (AMC) is the relative moisture of the pervious soil surfaces prior to the rainfall event and reflects the level of soil moisture in a five day interval preceding the rainfall extreme event. Antecedent Moisture is considered to be low when there has been little preceding rainfall and high when there has been considerable preceding rainfall prior to the extreme event. Determination of antecedent soil moisture content and classification into the antecedent moisture classes AMC I, AMC II and AMC III (Table 2), representing dry, average and wet conditions, is an essential matter for the application of the curve number procedure described next.

Table 2 Rainfall limits for AMC in growing season (Mockus, 1972).

AMC class	Total 5-day antecedent rainfall (mm): Growing season
I	Less than 36
II	36 to 53
III	More than 53
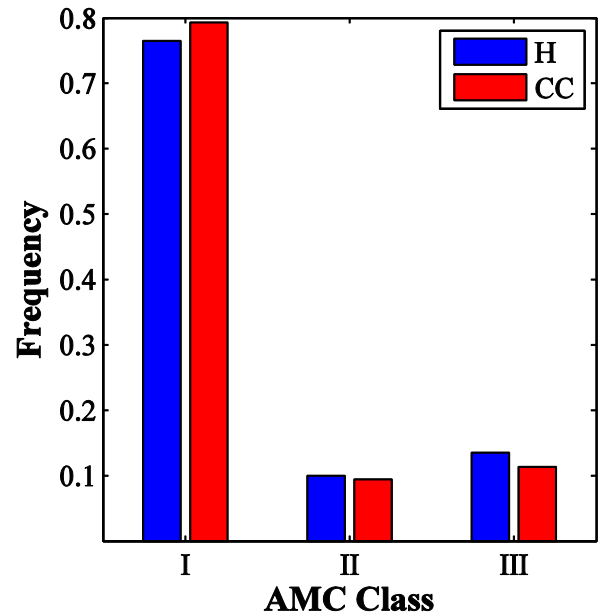
Figure 4. The histogram of the AMC classes for the growing season.

The rainfall time-series (both CC and H) are both post-processed in order to obtain the histogram of AMC classes calculated for the data series available.

Figure 4 illustrates such histogram calculated based on both H and CC.

No significant change in AMC can be observed between the two time-series. In this work, we considered watersheds to be AMC II, which is essentially an average moisture condition, even if there is a slightly higher likelihood for class III (Figure 4).

2.7 *The hazard curves*

The case-study neighborhood for micro-scale flood risk assessment is part of the Suna subward (Figure 5) in the Kinondoni District. Suna, located on the western bank of the Msimbazi river with an extension of about 50 ha, is a historically flood-prone area. The Msimbazi river flows across Dar es Salaam City from the higher areas of Kisarawe in the Coastal region and discharges into the Indian Ocean.
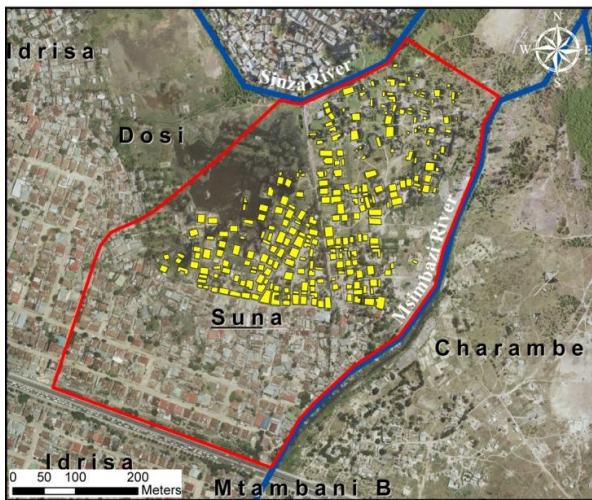
Figure 5. The case study area and the portfolio of the buildings studied.

The case-study area drains water from three different catchment areas (of about 250 km^2). The characteristics of the three catchments identified, the land-use and geological maps are described in detail in (DeRisi et al., unpubl.).

The peak flow in the three catchments is estimated by employing the Curve Number (CN) method (Mockus, 1972), with reference to six different return periods (e.g., 2, 10, 30, 50, 100 and 300-yr) based on both historical data (H) and climate projections (CC). The CN is representative of the catchment runoff capacity. If the terrain is moderately permeable and only a small portion of the water flows as run-off (e.g., the case of bare land and green areas), a CN corresponding to an AMC II (CN2) is usually used. If there is a high degree of urbanization (e.g., paved roads and high density of construction), the water over-flow can easily reach the main channel, a higher value of CN may be assigned (e.g., the CN corresponding to AMC III). In the following, the present condition is represented by CN2 (corresponding to AMCII). Meanwhile,

CN3 (corresponding to AMCIII) is used to describe the future territorial situation, based on a hypothetic urban expansion in the catchment area.

The inflow hydrographs (flooding discharge at the catchment's closing point) for catchment 1, that is the biggest among the three catchments, corresponding to two return periods (2 and 300-yr) and for two Curve Numbers (CN2 and CN3) are illustrated in Figure 6. It is possible to observe that for the same CN, the CC hydrographs are lower than those based on historical data (H). Changing the CN class there is a substantial increase in the discharge respect to the historical data of about 3.5 times for T_R=2 Ys and 2 times for T_R=300 Ys.
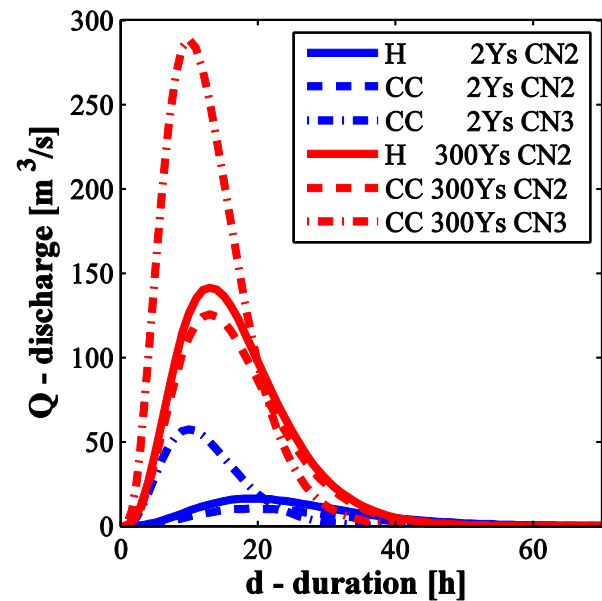
Figure 6. Hydrographs evaluated for catchment 1 (T_R= 2 and 300 years) with and without CC effects, for different CN classes.

The hydrographs are used next to obtain the inundation profile in terms of flood height and velocity for the nodes within the lattice for each return period T_R. The software FLO-2D was used for a bi-dimensional simulation of the flooding volume propagation (based on the calculated hydrographs and a digital elevation model, DEM) assuming a 45 hours simulation time (i.e., the total duration of the hydrograph). The detailed results for the specific case study in terms of inundation maps are shown in (DeRisi et al., unpubl.).

Starting from the inundation profile, using the procedure illustrated in (DeRisi et al., 2013) it is possible to obtain the hazard curves. These curves can be extracted for the centroid of each structure within the portfolio. The hazard curves, plotting the mean annual rate of exceeding various flooding heights (i.e., inverse of the return period), can be obtained based on CC and H. As a central statistics of the hazard curves for the portfolio of structures, the median hazard curve is calculated for each of the following three cases, namely, H CN2, CC CN2 and CC CN3 (Figure 7).

It is possible to observe that, for the same CN, the median hazard curves obtained based on historical data are very similar to those obtained considering the climate projections. Vice versa, considering the CN3, the hazard values obtained considering the climate projections are substantially larger (~one order of magnitude) with respect to the hazard curve calculated based on historical data only.
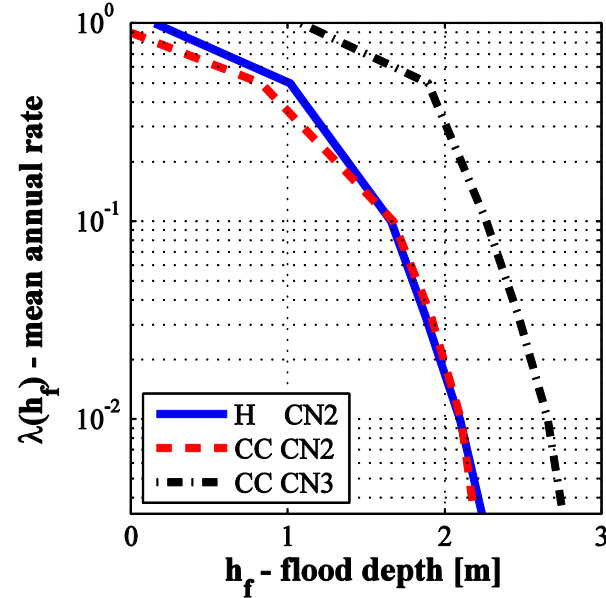
Figure 7. The mean annual rate of exceedance of a specific flood height (the median curves calculated over the entire lattice).

3 PORTFOLIO VULNERABILITY ASSESSMENT

In this work, a novel simulation-based and analytic methodology has been adopted for flood vulnerability assessment (DeRisi et al., unpubl., DeRisi et al., 2013). This methodology employs the Bayesian parameter estimation for calculating the structural fragility for a class of structures, by characterization of building-to-building variability and other sources of uncertainty based on a limited number of in-situ field surveys and remote-sensing. The portfolio of structures considered herein are a group of informal settlements located in Suna Subward, Dar es Salaam City. The following flooding actions are considered: hydrostatic pressure, hydrodynamic pressure and accidental debris impact.

The informal settlements located in this neighborhood reveal similar characteristics. For instance, they are all one-storey buildings, use cement stabilized bricks as wall material, and have a roof system made up of corrugated iron sheets and wooden beams. Moreover, the houses in this neighborhood, have similar geometrical patterns (the so-called Mozambique-style housing). As common adapting strategies, a significant portion of the inhabitants tend to build a barrier in front of the door or to build the house on a raised foundation (platform). The windows and doors are generally not water-tight.

3.1 The fragility assessment for the class

The fragility curves derived herein correspond to the Collapse limit state, defined as the critical flooding height in which the most vulnerable section of the most vulnerable wall in the building is going to break. The critical water height for structural collapse is calculated by employing structural analysis taking into account the various sources of uncertainties in geometry, material properties and construction details

For a prescribed limit state, the simulation procedure leads to a set of critical water height values. These critical water height values are used then as data in order to calculate, using Bayesian parameter estimation (Box and Tiao, 1992), the posterior probability distribution for the parameters of prescribed analytic fragility functions. Note that this posterior probability distribution can be interpreted as degrees of belief in the analytic fragility model that is defined based on a specific set of parameters. A large set of plausible analytic fragility curves can easily be simulated based on the posterior probability distribution derived. The set of simulated fragility curves can then be used in order to calculate various percentile fragility curves. Figure 8 below illustrates the 16th, 50th and 84th percentile fragility curves obtained for the Collapse limit state related to H with CN2. Note that the interval between the 16th and 84th percentile can be considered as a proxy for plus/minus one standard deviation confidence interval. The figure also illustrates the 50th percentile fragility curves for CC CN2 and CC CN3.

In fact, the fragility curves based on historical data only and the climate projections for different CN classes are not identical. This can be explained by the fact that velocity-dependent flooding action such as hydro-dynamic pressure and accidental debris impact are taken into account. However, as it can be observed, CC CN2 and CC CN3 fragility curves are contained within the confidence interval for H CN2.

4 FLOOD RISK ASSESSMENT

The flooding risk λ_{ls} expressed as the mean annual rate of exceeding a given limit state ls can be calculated as:

$$\lambda_{ls} = \int_{h_f} P\left(ls \mid h_f\right) \cdot \left| d\lambda\left(h_f\right) \right| \tag{3}$$

where h_f denotes the flooding height at a given point in the considered area. $P(ls|h_f)$ denotes the flooding fragility for limit state ls expressed in term of the conditional probability of exceeding the limit

state threshold given flooding height. Point estimates of the flooding risk can be obtained by integrating the robust fragility for the class of structures considered and the flood hazard in Eq. (3).

The annual probability of exceeding a limit state $P(ls)$, assuming a homogeneous Poisson process model with rate λ_{ls}, can be calculated as:

$$P(ls) = 1 - \exp(-\lambda_{ls}) \qquad (4)$$

The exposure to risk can be quantified by calculating the total expected loss or the expected number of people affected for the portfolio of buildings.
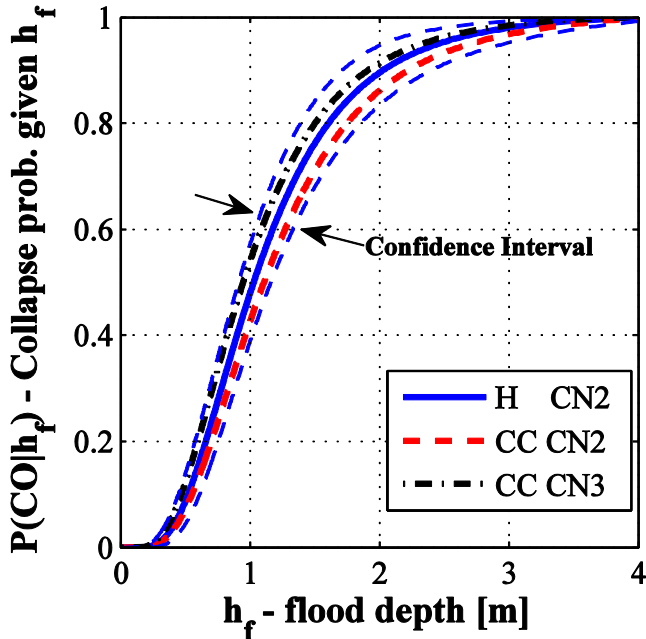
Figure 8. The fragility curves for the CO limit state (based on 20 simulations).

4.1 Estimating the exposure

The expected repair costs (per building or per unit residential area), $E[R]$, can be calculated as a function of the limit state probabilities and by defining the damage state i as the structural state between limit states i and $i+1$:

$$E[R] = \sum_{i=1}^{N_{ls}} \left[P(ls_{i+1}) - P(ls_i) \right] \cdot R_i \qquad (5)$$

where N_{ls} is the number limit states that are used in the problem in order to discretize the structural damage; R_i is the repair cost corresponding to damage state i; and $P(ls_{N_{ls}+1}) = 0$. The expected number of people affected by flooding can also be estimated as a function of the limit state probabilities from Eq. (5) replacing R_i by the population density (per house or per unit residential area).

4.2 Results

Figure 9 illustrates the expected value of the number of people endangered by flooding per year and per house-hold, taking into account only the col-lapse limit state probabilities in Eq. 5 (based on only historical data, CN2 class).
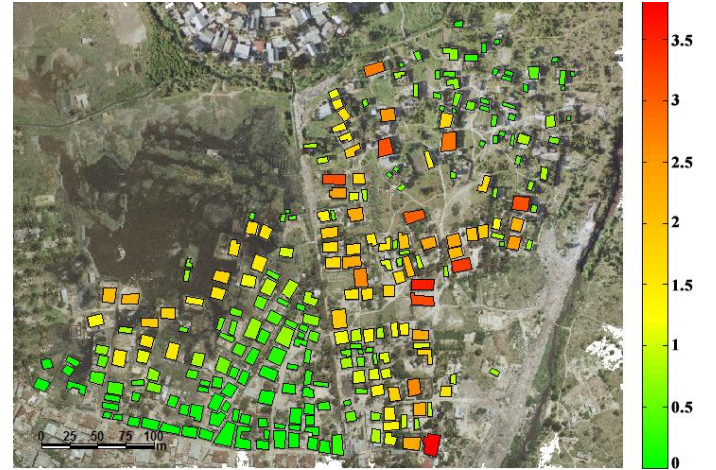
Figure 9. The house-hold risk map: number of people affected (CO limit state only).

Table 3 reports the total annual expected replacement costs (collapse limit state only) normalized to the total replacement cost for the entire portfolio, considering both the historical data H and the climate change projections CC, based on two different land-cover scenarios (CN2 and CN3). It can be observed that CC and the CN3 class (un-controlled urbanization) might lead to an increase of about 30% in the expected annual replacement costs.

Table 3. Expected losses (CO)

	F - σ	F	F + σ
H CN2	36%	33%	30%
CC CN2	30%	28%	25%
CC CN3	66%	63%	60%

5 CONCLUSION

A performance-based analytic procedure for micro-scale flood risk assessment for a portfolio of informal settlements in DSM is presented. This procedure has a modular structure and consists of, climate modeling (based on climate projections and historical data), flood hazard assessment, portfolio vulnerability assessment and point-wise risk assessment. It can be observed that assuming the same land-cover characteristics between present and the future (within around 50 years), the effect of climate change for DSM is not significant for the particular climate scenario considered (RCP8.5). However, pairing up the climate projections with a un-controlled urban expansion scenario for the city (i.e., a much more impervious terrain), leads to around 30% increase in overall exposure to flooding in the neighborhood studied (assuming that the buildings' characteristics are going to remain the same).

REFERNCES

Alley, R., Berntsen, T., Bindoff, N. L., Chen, Z., Chidthaisong, A., Friedlingstein, P., Gregory, J., Hegerl, G., .Heimann, M. & Hewitson, B. 2007. IPCC 2007: summary for policymakers. *Climate Change*, 1-18.

Bellucci, A., Bucchignani, E., Gualdi, S., Mercogliano, P., Montesarchio, M. & Scoccimarro, E. 2012. Data for global climate simulations available for downscaling. *CLUVA project - Climate Change and Urban Vulnerability in Africa.*

Box, G. E. P. & Tiao, G. C. 1992. *Bayesian Inference in Statistical Analysis*, John Wiley & Sons, Inc.

Connolly, R. D., Schirmer, J. & Dunn, P. K. 1998. A daily rainfall disaggregation model. *Agricultural and Forest Meteorology, 92*, 105-117.

DeRisi, R., Jalayer, F., DePaola, F., Iervolino, I., Giugni, M., Topa, M. E., Mbuya, E., Kyessi, A., Manfredi, G. & Gasparini, P. unpubl. Flood Risk Assessment for Informal Settlements, Under Review. *Natural Hazards.*

DeRisi, R., Jalayer, F., Iervolino, I., Manfredi, G. & Carozza, S. 2013. VISK: a GIS-compatible platform for micro-scale assessmen of flooding risk in urban areas. *In:* Papadrakakis, M., Papadopoulos, V. & Plevris, V. (eds.) *COMPDYN, 4th ECCOMAS Thematic Conference on Computational Methods in Structural Dynamics and Earthquake Engineering.* Kos Island, Greece.

Gualdi, S., Somot, L., Li, L., Artale, V., Adani, M., Bellucci, A., Braun, A.-., Calmanti, S., Carillo, A., Dell'Aquila, A., Deque, M., Dubois, C., Elizade, A., Harzallah, A., Jacob, D., L'Hévéder, D., May, W., Oddo, P., Ruti, P., Sanna, A., Sannino, G., Scoccimarro, E., Savault, F. & Navarra, A. 2013. The CIRCE simulations: Regional Climate Change Projections with Realistic Representation of the Mediterranean Sea. *Bullettin of American Meteorological Society*, 65-81.

Güntner, A., Olsson, J., Calver, A. & Gannon, B. 2001. Cascade-based disaggregation of continuous rainfall time series: the influence of climate. *Hydrology and Earth System Sciences Discussions, 5*, 145-164.

Hoyois, P. & Guha-Sapir, D. 2012. Measuring the Human and Economic Impact of Disasters. Center for Research on the Epidemiology of Disaster.

Jonkman, S. N., Vrijling, J. K. & Vrouwenvelder, A. C. W. M. 2008. Methods for the estimation of loss of life due to floods: a literature review and a proposal for a new method. *Natural Hazards, 46*, 353-389.

Kang, J., Su, M. & Chang, L. 2005. Loss functions and framework for regional flood damage estimation in residential area. *Journal of Marine Science and Technology, 13*, 193-199.

Kelman, I. 2002. *Ph.D Thesis: Physical flood vulnerability of residential properties in coastal, eastern England.* University of Cambridge.

Khan, S. & Kelman, I. 2011. Progressive climate change and disasters: connections and metrics. *Natural Hazards, 61*, 1477-1481.

Mockus, V. 1972. National engineering handbook, Section 4, hydrology. *US Soil Conservation Service, Washington, DC.*

Nadal, N. C., Zapata, R. E., Pagán, I., López, R. & Agudelo, J. 2009. Building damage due to riverine and coastal floods. *Journal of Water Resources Planning and Management, 136*, 327-336.

Olsson, J. 1998. Evaluation of a scaling cascade model for temporal rain-fall disaggregation. *Hydrology and Earth System Sciences Discussions, 2*, 19-30.

Pistrika, A. & Tsakiris, G. 2007. Flood risk assessment: A methodological framework. *Water Resources Management: New Approaches and Technologies. European Water Resources Association, Chania, Crete-Greece.*

Rebora, N., Ferraris, L., vonHardenberg, J. & Provenzale, A. 2006. RainFARM: Rainfall downscaling by a filtered autoregressive model. *Journal of Hydrometeorology, 7*, 724-738.

Rockel, B., Will, A. & Hense, A. 2008. The regional climate model COSMO-CLM (CCLM). *Meteorologische Zeitschrift, 17*, 347-348.

Schwarz, J. & Maiwald, H. 2012. Empirical vulnerability assessment and damage for description natural hazards following the principles of modern macroseismic scales. *14th WCEE - World Conference of Earthquake Engineering.* Lisboa, Portugal.

Smith, D. 1994. Flood damage estimation- A review of urban stage-damage curves and loss functions. *Water S. A., 20*, 231-238.

UN-HABITAT 2010. State of the World's Cities 2010/2011 - Cities for All: Bridging the Urban Divide. *State of the World's Cities.*

WCRP. 2008. *World Climate Research Programme, CMIP5 Coupled Model Intercomparison Project* [Online]. Available: http://cmip-pcmdi.llnl.gov/cmip5/.